Systems/Circuits

# Resting-State fMRI-Based Screening of Deschloroclozapine in Rhesus Macaques Predicts Dosage-Dependent Behavioral Effects

**Atsushi Fujimoto,[1*] Catherine Elorette,[1*] J. Megan Fredericks,[1] Satoka H. Fujimoto,[1] Lazar Fleysher,[4] Peter H. Rudebeck,[1†] and Brian E. Russ[1,2,3†]**

[1]Nash Family Department of Neuroscience and Friedman Brain Institute, Icahn School of Medicine at Mount Sinai, New York, New York 10029, [2]Center for Biomedical Imaging and Neuromodulation, Nathan Kline Institute, Orangeburg, New York 10962, [3]Department of Psychiatry, New York University at Langone, New York, New York 10016, and [4]BioMedical Engineering and Imaging Institute, Icahn School of Medicine at Mount Sinai, New York, New York 10029

**Chemogenetic techniques, such as designer receptors exclusively activated by designer drugs (DREADDs), enable transient, reversible, and minimally invasive manipulation of neural activity *in vivo*. Their development in nonhuman primates is essential for uncovering neural circuits contributing to cognitive functions and their translation to humans. One key issue that has delayed the development of chemogenetic techniques in primates is the lack of an accessible drug-screening method. Here, we use resting-state fMRI, a noninvasive neuroimaging tool, to assess the impact of deschloroclozapine (DCZ) on brainwide resting-state functional connectivity in 7 rhesus macaques (6 males and 1 female) without DREADDs. We found that systemic administration of 0.1 mg/kg DCZ did not alter the resting-state functional connectivity. Conversely, 0.3 mg/kg of DCZ was associated with a prominent increase in functional connectivity that was mainly confined to the connections of frontal regions. Additional behavioral tests confirmed a negligible impact of 0.1 mg/kg DCZ on socio-emotional behaviors as well as on reaction time in a probabilistic learning task; 0.3 mg/kg DCZ did, however, slow responses in the probabilistic learning task, suggesting attentional or motivational deficits associated with hyperconnectivity in fronto-temporo-parietal networks. Our study highlights both the excellent selectivity of DCZ as a DREADD actuator, and the side effects of its excess dosage. The results demonstrate the translational value of resting-state fMRI as a drug-screening tool to accelerate the development of chemogenetics in primates.**

*Key words:* **deschloroclozapine; DREADDs; functional connectivity; ICA; macaque monkey; rs-fMRI**

### Significance Statement

**Chemogenetics, such as designer receptors exclusively activated by designer drugs (DREADDs), can afford control over neural activity with unprecedented spatiotemporal resolution. Accelerating the translation of chemogenetic neuromodulation from rodents to primates requires an approach to screen novel DREADD actuators *in vivo*. Here, we assessed brainwide activity in response to a DREADD actuator deschloroclozapine (DCZ) using resting-state fMRI in macaque monkeys. We demonstrated that low-dose DCZ (0.1 mg/kg) did not change whole-brain functional connectivity or affective behaviors, while a higher dose (0.3 mg/kg) altered frontal functional connectivity and slowed response in a learning task. Our study highlights the excellent selectivity of DCZ at proper dosing, and demonstrates the utility of resting-state fMRI to screen novel chemogenetic actuators in primates.**

Received Feb. 15, 2022; revised Apr. 15, 2022; accepted Apr. 29, 2022.

Author contributions: A.F., C.E., P.H.R., and B.E.R. designed research; A.F., C.E., J.M.F., S.H.F., and L.F. performed research; A.F., C.E., J.M.F., P.H.R., and B.E.R. analyzed data; A.F., C.E., P.H.R., and B.E.R. wrote the first draft of the paper; A.F., C.E., J.M.F., S.H.F., L.F., P.H.R., and B.E.R. edited the paper; A.F., C.E., P.H.R., and B.E.R. wrote the paper.

A.F., C.E., B.E.R., and P.H.R. were supported by National Institute of Mental Health and the BRAIN Initiative Grants R01MH110822 and R01MH117040. B.E.R. was supported by National Institute of Mental Health Grant R01MH111439 and National Institute of Neurological Disorders and Stroke Grant R01NS109498. A.F. was supported by Takeda Science Foundation Overseas Research Fellowship and Brain & Behavior Research Foundation Young Investigator Grant 28979. We thank Dr. Paula Croxson for providing the foundation on which this work was built; Jairo Munoz and Niranjana Bienkowska for assistance with data acquisition; and Drs. Paul Taylor and Alex Franco for help with fMRI data preprocessing and analysis, respectively.

*A.F. and C.E. contributed equally to this work.

†P.H.R. and B.E.R. contributed equally to this work as joint last authors.

The authors declare no competing financial interests.

Correspondence should be addressed to Brian E. Russ at brian.russ@mssm.edu.

https://doi.org/10.1523/JNEUROSCI.0325-22.2022

## Introduction

The development of chemogenetics, such as designer receptors exclusively activated by designer drugs (DREADDs), has ushered in a new era of neuroscience research. DREADDs use a family of modified G-protein coupled muscarinic cholinergic receptors to modulate neural activity *in vivo* (Armbruster et al., 2007). In rodents, DREADDs have been instrumental for identifying the function of specific cell populations and neural circuits (Stachniak et al., 2014; Roth, 2016). The development of DREADDs in primates has been slower for a number of reasons (Fredericks et al., 2019) but holds the promise of enabling the translation of chemogenetic methods to treat psychiatric and neurologic disorders.

DREADD receptors alter the membrane potential of neurons only when bound by nonendogenous ligands (Roth, 2016). Recently, deschloroclozapine (DCZ) has been identified as a selective and high-affinity activator for muscarinic-based DREADDs with few off-target effects, unlike the original actuator clozapine-N-oxide (Gomez et al., 2017; Nagai et al., 2020; Roseboom et al., 2021; Rodd et al., 2022). At a dose of 0.1 mg/kg, DCZ occupies up to 80% of DREADD receptors *in vivo* (Nagai et al., 2020), producing rapid and robust changes in neural activity and alterations in behavior. Despite this, there are open questions that could limit the appropriateness of DCZ for use in both basic and clinical settings.

First, it is unclear how DCZ, in the absence of DREADDs, impacts brainwide patterns of neural activity. This is potentially vital for discerning the more subtle effects of systemic DCZ on the brain, such as changes in functional connectivity between brain areas, information essential for assessing the clinical appropriateness of DCZ. Second, while 0.1 mg/kg DCZ has little impact on tasks that assess executive function or motivation (Nagai et al., 2020; Upright and Baxter, 2020), it is unknown whether the same dose causes changes in translationally relevant affective tasks. While DCZ has negligible affinity for most endogenous receptors, it has some affinity to mAchRs and serotonin Type 2 receptors that are primarily located in the cortex (Varastet et al., 1992; Barnes and Sharp, 1999) and that are potentially important for affective behaviors (Nagai et al., 2020). It is possible, therefore, that even at low, but functionally relevant doses, DCZ may impact affective behavior by binding to these endogenous receptors. Addressing these issues in macaque monkeys is critical as marked changes in brainwide activity patterns, behavior, or both would limit the usefulness of DCZ as the actuator in basic neuroscience and in future clinical settings.

Here we addressed these questions using resting-state fMRI (rs-fMRI) and behavioral assessments in macaque monkeys. We measured the impact of either vehicle, low-dose DCZ (0.1 mg/kg), or high-dose DCZ (0.3 mg/kg) on whole-brain functional connectivity as well as in conditioned and unconditioned tasks that assess socio-emotional processing. We found no changes in overall functional connectivity or affective behavior after administration of vehicle or 0.1 mg/kg of DCZ. Conversely, higher doses of DCZ at 0.3 mg/kg affected brainwide patterns of functional connectivity, in particular in the connections of frontal regions to the temporal and parietal lobes. This dose also impacted decision-making in a probabilistic learning task, increasing reaction times (RTs). Thus, our experiments reveal the dosage-dependent impact of DCZ on brainwide functional connectivity and demonstrate the potential value of rs-fMRI as an additional drug-screening tool in basic and clinical neuroscience.

## Materials and Methods

### *Subjects*

Seven adult rhesus macaques (*Macaca mulatta*) served as subjects (6 males and 1 female, 7-8 years old). All subjects underwent anesthetized fMRI scans, while subsets of 4 and 3 animals were assessed in 2 socio-emotional tasks and a probabilistic learning task, respectively (see Table 1). All procedures were reviewed and approved by the Icahn School of Medicine Animal Care and Use Committee.

### *fMRI data acquisition*

Animals were first sedated with ketamine (5 mg/kg) and dexmedetomidine (0.0125 mg/kg) at least 1.5 h before the data collection to prevent detrimental effects of ketamine on neural activities. They were then intubated and maintained under low level (0.7%-0.8%) isoflurane throughout the session to ensure preservation of resting-state networks (Hutchison et al., 2013; Wu et al., 2016; Giacometti et al., 2021). During all scanning sessions, anesthetized macaques were contained within a primate chair in the sphinx position with their heads supported by a sling. Because animals were not held in a stereotactic frame, this meant we were able to maintain sedation with lower levels of anesthesia than is often used. To minimize the effect of physiological changes in the neural activity, vital signs (end-tidal $CO_2$, body temperature, blood pressure, capnograph) were continuously monitored and maintained as steadily as possible throughout an experimental session. Structural and functional scans were collected each session, as well as pre-injection (baseline) and post-injection (DCZ or vehicle) functional scans. First, a set of setup scans were acquired, which included shimming based on the acquired fieldmap. Additionally, a 3D T1-weighted image (0.5 mm isotropic, TR/TE 2500/2.81 ms, flip angle 8°) was acquired. Following monocrystalline iron oxide nanoparticle (MION) injection (i.v.) (Leite et al., 2002; Russ et al., 2021), three or four runs of EPI functional scans (1.6 mm isotropic, TR/TE 2120/16 ms, flip angle 45°, 300 volumes per each run) were obtained for baseline functional resting states. Then, ~30 min from the beginning of the pre-injection rs-fMRI data collection, either DCZ (0.1 or 0.3 mg/kg) or vehicle was administered (i.v.), and subsequently an additional three or four functional runs (with the same parameters) were collected. Test EPI data were collected ~15 min after DCZ or vehicle injection to ensure trafficking of the drug to the brain (Nagai et al., 2020). The order of drug condition was counterbalanced across animals. Three animals (Bu, Cy, Wo) completed all the drug conditions while the other animals did not (Table 1). This was the case as some of the animals included in these analyses were scheduled for other studies where DREADDs would be expressed in the brain and thus precluded them from further study.

### *Unconditioned socio-emotional tasks*

Four animals (Wo, He, La, Ha) were tested on two well-validated behavioral tasks that assess socio-emotional function: the human intruder (Kalin and Shelton, 1989) and social interaction tests (Kling and Cornell, 1971). Behavioral tests were conducted following injections of either vehicle (2% DMSO in saline) or 0.1 mg/kg DCZ. Injections were given intramuscularly 30-60 min before behavioral testing in keeping with the known pharmacokinetics of DCZ (Nagai et al., 2020). Three of the animals received vehicle treatments before low-dose DCZ treatments, and a fourth animal received low-dose DCZ treatment before vehicle. Each animal was tested only once in each drug condition for each behavioral test. All behavioral data were scored offline in Observer XT version 14.0 (Noldus).

*Human intruder.* Animals were tested on a human intruder paradigm, which has been shown to accurately assess anxiety behaviors in macaques (Kalin and Shelton, 1989; Kalin et al., 2001, 2007; Izquierdo et al., 2007). Testing was conducted in a Wisconsin General Testing Apparatus. The sliding doors of the Wisconsin General Testing Apparatus were left open so the animal could observe the room throughout the test session. We have adapted our testing procedure and behavioral ethogram from a previous study (Raper et al., 2019).

The paradigm consisted of three conditions (alone, profile, stare) presented in the same order to all monkeys for a total duration of 30 min. The experimenter wore a rubber mask depicting a different

**Table 1. Assignments of monkeys to fMRI and behavioral testing conditions[a]**

| Animal | rs-fMRI (vehicle) | rs-fMRI (DCZ 0.1 mg/kg) | rs-fMRI (DCZ 0.3 mg/kg) | Socio-emotional tasks | Probabilistic learning task |
|---|---|---|---|---|---|
| La | N | Y | N | Y | N |
| Ha | N | Y | N | Y | N |
| Wo | Y | Y | Y | Y | Y |
| He | N | Y | Y | Y | Y |
| Cy | Y | Y | Y | N | Y |
| Bu | Y | Y | Y | N | N |
| Pi | Y | N | Y | N | N |

[a]Y and N indicate the condition that the data were collected and not collected, respectively.

human male face during each testing session, presented in pseudorandom order to subjects with no repetitions of masks per subject. Different colored curtains hung behind the experimenter's seat were also used to increase novelty. Within each testing session, monkeys were first left alone to observe the room and acclimatize to the environment (alone condition). Next, the experimenter, wearing a novel mask, stepped into the animal's FOV with only their profile visible to the animal, then sat in a chair at the eye level of the animal for the duration of the condition. The experimenter remained still, with only the profile visible, for 9 min (profile condition). Another alone condition elapsed for 3 min to allow the animal to return to baseline behavior, before the experimenter stepped back into view, then sat in a chair at eye level facing the animal and making eye contact. The experimenter remained still, attempting to make eye contact with the animal for 9 min (stare condition) before stepping out of view and ending the session. A minimum of 1 month elapsed between repetitions of this task with the same animal, as animals may habituate to the human intruder (Kalin and Shelton, 1989).

*Social interaction.* Animals were removed from the home cage and placed in a play cage set up in an unfamiliar room. A familiar cagemate was introduced to the play cage, and social interaction between the subject and cagemate was observed. We used an ethogram previously defined by others to evaluate social behaviors (Wellman et al., 2016; Forcelli et al., 2017). The cagemate chosen for this task was always the same across conditions. The cagemate did not receive any injection before testing. A minimum of 48 h elapsed between social interaction tests.

*Probabilistic stimulus-reward learning task*

Three monkeys (He, Cy, and Wo) were trained to perform a two-alternative forced-choice probabilistic learning task on a touch-sensitive monitor. All testing occurred while monkeys were seated in a wheeled transport cage. In each 200 trial session, subjects had to learn to discriminate which visual stimulus in two pairs of novel stimuli was associated with the highest probability of receiving a food reward pellet. Food reward pellets were an equal mix of banana, grape, and raspberry flavored 190 mg Purified Non-Human Primate Tablets (TestDiet product 5TUQ). The different pellets were mixed in together in equal quantity, so the flavor delivered on each trial was random. This was the same for both pairs of stimuli. In each pair of stimuli, one option was associated with an 80% probability of receiving a reward, whereas the other was associated with 20% probability of receiving a reward. Stimuli were novel at the beginning of each session; the assignment of visual stimuli to high/low probability was random. The probability of receiving a reward was fixed throughout the session; and at the completion of the session, a "lunch box" containing the majority of the subjects' food for the day was opened.

Each trial began with the presentation of a centrally located green square "lever" stimulus. Once monkeys pressed the lever stimulus, two stimuli were presented to the left and right of the screen, and monkeys could choose between them. Pressing one stimulus caused the nonselected option to be removed from the screen. The chosen stimulus remained on the screen for a further 0.5 s before being extinguished and a 4 s intertrial interval commenced. For one pair of stimuli, if a reward was to be delivered, it was dispensed when the chosen stimulus was removed from the screen. For the other pair of stimuli, if a reward was to be delivered, it was dispensed 1 s after the chosen stimulus was removed from the screen. The presentation of stimuli pairs was randomized across trials, and the left-right location of each stimulus was also counterbalanced across trials. Once a trial started, the lever stimulus or the two choice options stayed on the screen until monkeys made a response. If a monkey failed to complete >20 trials in 30 min after starting the session, the session was aborted. In practice, no sessions were aborted, as all monkeys completed their testing sessions within ~30 min.

Monkeys completed daily 200 trial sessions (100 trials of each pair), run 4-5 d per week. 0.1 mg/kg, 0.3 mg/kg DCZ, and vehicle were administered in sessions after stable performance was established each week. Only one session where DCZ was administered was run per week, and vehicle and DCZ sessions were always separated by at least 1 d. In practice, this meant that injections of 0.1 mg/kg, 0.3 mg/kg DCZ, or vehicle were administered on Wednesday, Thursday, or Friday. An example of a week's testing schedule is as follows: baseline testing with no injection on Monday, Tuesday, Thursday; vehicle administered Wednesday; and 0.1 mg/kg DCZ administered on Friday. Subjects each completed three sessions following administration of vehicle, 0.1, and 0.3 mg/kg DCZ. On each daily session, DCZ or vehicle was injected (i.m.) 30-60 min before testing.

*Drug preparation*

To prepare a DCZ solution for fMRI or socio-emotional testing, DCZ powder (HY-42110, MedChemExpress) was dissolved in DMSO (2% of total volume) and then diluted in saline to a concentration of 0.1 or 0.3 mg/kg, with a total volume of 1 ml. Vehicle solution was prepared as 2% DMSO diluted in 1 ml saline. One vehicle scan was conducted without DMSO (Monkey Wo). Both solutions underwent a sterilized filter (0.22 μm) before injection. DCZ or vehicle solution was prepared within 30 min of usage.

For the probabilistic learning testing, both vehicle and DCZ were prepared using sterile procedures and previously published drug preparation approaches for behavioral testing in macaques (Upright and Baxter, 2020). The vehicle consisted of 0.5% acetic acid, 50% 1 M sodium acetate, and 49.5% 0.2 M NaOH. Each solution of DCZ or vehicle ultimately had a pH between 5.5 and 6.0. When DCZ was administered, the drug was first dissolved in acetic acid and sodium acetate and then diluted with NaOH. The vehicle remained consistent across both drug doses (0.1 or 0.3 mg/kg of DCZ). However, the concentration of each dose was altered so the total volume of each injection was the same no matter the dose (e.g., a 0.1 mg/kg dose had a concentration of 1 mg/ml), while a 0.3 mg/kg dose had a concentration of 3 mg/ml. As with fMRI testing, DCZ or vehicle solution was prepared within 30 min of usage.

*fMRI analysis*

Functional imaging data were preprocessed with standard AFNI/SUMA pipelines (Cox, 1996; Jung et al., 2021). Raw images were first converted into NIFTI data file format and ordered into BIDS format (Gorgolewski et al., 2016). The T1-weighted image from each session was first warped to the standard NMT atlas space using a newly developed macaque skull stripping function followed by AFNI's @animal_warper command (Seidlitz et al., 2018; Jung et al., 2021). Specifically, the T1-weighted images were spatially normalized, then skull-stripped using the U-Net model built from Primate Data-Exchange open datasets (Wang et al., 2021), the mask was dilated out 6 mm to ensure the whole brain was within the mask, and finally the mask was applied to the original image, which was then renormalized. This normalized skull-stripped T1-weighted image was then aligned to the NMT atlas (Seidlitz et al., 2018), along with subject-specific versions of the CHARM (Jung et al., 2021) and SARM atlases (Hartig et al., 2021).

The EPI data were preprocessed using a customized version of the AFNI NHP preprocessing pipeline (Jung et al., 2021). For each session, pre- and post-injection data were processed separately using the same parameters. In addition to a set of dummy scans, the first three TRs of each EPI were removed to ensure that any magnetization effects were removed from the data before functional connectivity analyses. The images were first slice time corrected, then motion correction was

**Table 2. Behavioral ethogram for human intruder task[a]**

| Category and specific behaviors | Measurement | Examples |
|---|---|---|
| Affiliative | Cumulative frequency | |
| Lipsmack | Frequency | Rapid movement of pursed lips, accompanied by a smacking sound |
| Present | Frequency | Rigid posture (knees locked) with tail elevated and rump oriented toward the stimulus object |
| Anxiety | Cumulative frequency | |
| Scratch | Frequency | Rapid scratch of body with hands or feet |
| Body shake | Frequency | Shake of the whole body or just head and shoulders region |
| Tooth grind | Frequency | Repetitive rubbing or chewing of upper and lower teeth |
| Yawn | Frequency | Open mouth widely, exposing teeth |
| Fearful | Cumulative frequency | |
| Withdrawal | Frequency | Quick, jerky motion away from the stimulus object (jump back) |
| Grimace | Frequency | Retracted lips, exposed clenched teeth |
| Hostile | Cumulative frequency | |
| Cage aggression | Frequency | Slaps, shakes, bites, or slams body against cage |
| Threat | Frequency | Open mouth (no teeth exposed) |
| Bark | Frequency | Low pitch, high intensity, rasping, guttural |
| Lunge | Frequency | A quick, jerky movement toward the stimulus |
| Position | Duration | |
| Front of cage | Duration | No part of animal's body contacts back of the cage |
| Back of cage | Duration | Animal's body contacts back of the cage |
| Stereotypies | Cumulative Duration | |
| Pacing | Duration | Repetitive motor pattern around the test cage |
| Motor stereotypy | Duration | Repetitive, abnormal voluntary or involuntary motor patterns (e.g. swinging, twirling, flipping) |
| Stillness | Duration | Motionless posture for at least 3 s (except small head movements) |
| Vocalizations | Cumulative frequency | |
| Coo | Frequency | Clear soft pitch and intensity, sounds like "ooooh" |
| Scream | Frequency | High pitch, high intensity screech or loud chirp |

[a]Adapted from Raper et al. (2019).

**Table 3. Behavioral ethogram for social interaction task[a]**

| Category and specific behaviors | Measurement | Examples |
|---|---|---|
| Avoidance | Cumulative frequency | |
| Attack | Frequency | Makes threatening gestures (i.e., mouth threat, head or body lunge, cage shake) toward or hits, grabs, or bites the conspecific |
| Cower | Frequency | Withdraws from the conspecific in a crouched or recoiled position |
| Escape | Frequency | Sudden, explosive movement away from conspecific |
| Withdrawal | Frequency | Moves away at a normal pace from the conspecific when approached |
| Movement | Cumulative duration | |
| Passive | Duration | Inactive, stays in one location |
| Manipulation | Duration | Handles, chews, licks, moves, or smells objects or cage parts |
| Locomotion | Duration | Walks, runs, climbs, or jumps |
| Self-directed | Duration | Engages in self-directed behaviors |
| Social contact | Cumulative duration | |
| Contact | Duration | Touches or holds the conspecific, not covered by any other behavior |
| Gives grooming | Duration | Subject grooms the conspecific |
| Receives grooming | Duration | The conspecific grooms the subject |
| Play | Duration | Chasing, wrestling, and "rough and tumble" behaviors |

[a]Adapted from Forcelli et al. (2017).

applied and the EPIs were aligned to the within session T1-weighted image and warped to the standard space. Following alignment to the standard space, the EPIs were blurred with an FWHM of 3 mm, and then converted to percent signal change. We then regressed the motion derivatives from each scan along with cerebrospinal fluid and white matter signal regressors. The residuals of this analysis were then used to compute the functional connectivity analysis described below.

The full connectome analyses were computed using 3dNetCorr function in AFNI (Cox, 1996; Taylor and Saad, 2013). The error time series from the preprocessing steps described above were split into half runs, and then we computed the correlation between ROIs at various levels of the cortical (Jung et al., 2021) and subcortical (Hartig et al., 2021) hierarchical atlas. Following the creation of the individual correlation matrices, or connectomes, for each half run, the connectomes were Fisher's $z$-transformed and then averaged within condition to create mean connectomes for each condition (both pre-/post-injection for the vehicle, DCZ 0.1 mg/kg, and DCZ 0.3 mg/kg sessions) at all hierarchical levels. We then calculated the difference between connectomes by subtracting the pre-injection data from the post-injection data for each session. Finally, the average difference connectome was computed across subjects for each drug level. To statistically determine the effect of drug on the functional connectivity in CHARM and SARM atlases, the mean connectomes from individual monkeys were then submitted to an ANOVA with main effects of drug and area category. Monkey and brain area were modeled as random effects, and brain area was nested under monkey.

In addition to the functional connectomes analyses, we used a modified group independent components analysis (ICA) to look for any changes in the component structure of our data following the drug manipulations. The same split run error time series from the connectome analyses were submitted to FSL's melodic ICA function (Beckmann and Smith, 2004; Beckmann et al., 2009) allowing for 30 possible components and a mixture

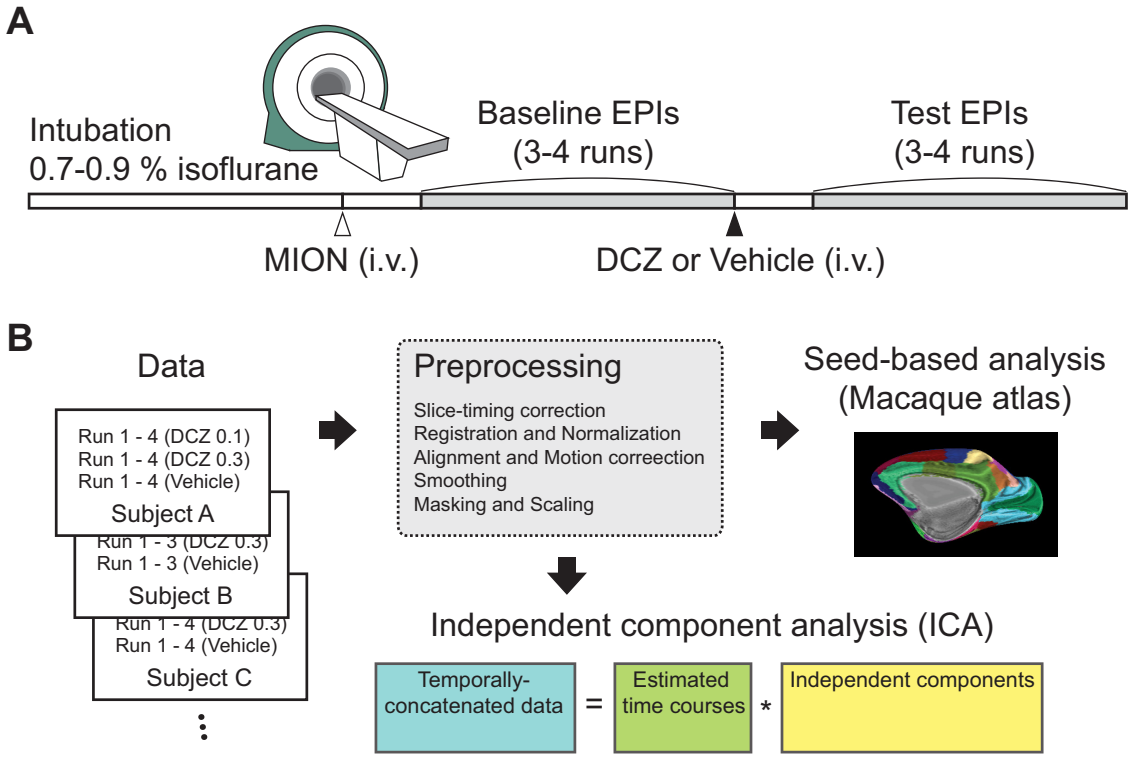


**Figure 1.** Schematic of experiments. ***A***, An imaging session. Subjects were lightly anesthetized with isoflurane gas throughout a session. A contrast agent (monocrystalline iron oxide nanoparticle [MION], 10 mg/kg) was administered intravenously before functional scans. Drug (vehicle, 0.1 mg/kg DCZ, or 0.3 mg/kg DCZ) was prepared and systemically administered (i.v.) following baseline scans, and test scans were acquired after 15 min of drug injection. ***B***, Data analysis pipeline. The scan data for each session initially went through preprocessing procedures. Then seed-based analysis was performed using predetermined ROIs based on the CHARM and SARM atlases. The temporally concatenated scan data across all sessions were used for ICA.

model threshold of 0.5. Following the computation of the group ICA, we submitted resultant data to FSL's dual regression function, which was used to extract the spatial ICs for each subject and condition (Beckmann et al., 2009; Nickerson et al., 2017). The extracted condition IC scores were then submitted to a 2 (Pre-Injection vs Post-Injection) × 3 (Drug: Vehicle, DCZ 0.1 mg/kg, DCZ 0.3 mg/kg) ANOVA, which was computed on a voxel × voxel basis.

*Behavioral analysis*

Data from socio-emotional tests were assessed by a scorer blinded to the condition. Data were scored in Observer XT 14.0 and exported to GraphPad Prism 9.0. Behavioral ethograms (Tables 2 and 3) were adapted from previous studies (Forcelli et al., 2017; Raper et al., 2019). Behavioral responses in the human intruder and social interaction paradigms were assessed for normality using a Shapiro–Wilk normality test. Human intruder data were analyzed using two-way repeated-measures ANOVAs with matching by subject. No assumption of sphericity was made. Sidak's multiple comparison test was used to evaluate differences between categories (i.e., differences between DCZ and vehicle treatments within the alone, profile, and stare conditions). Hostile and anxious behaviors during the stare condition of the human intruder test were analyzed using a paired Student's *t* test, with matching by subject. Social interaction data were also analyzed using a paired Student's *t* test, with matching by subject.

Data from the probabilistic learning task were analyzed using MATLAB 2021a (The MathWorks). In all sessions analyzed, each of the monkeys learned to discriminate the pairs of stimuli by the end of the session. This was based on a running average of 10 trials, and criterion was set at 8 of 10 trials, or 80%. We assessed RT as a measure of general task-execution process, such as attention or motivation. RT was defined as the time duration (in milliseconds) from the presentation of two stimuli to a choice response of the monkeys. We analyzed RT using ANOVA with factors of drug as a main effect and monkey and session as random effects.

## Results

### The impact of low- and high-dose DCZ on brainwide fMRI functional connectivity

Seven subjects underwent anesthetized fMRI scanning using isoflurane levels below those shown to adversely impact functional connectivity in frontal cortex (Hutchison et al., 2013; Wu et al., 2016; Giacometti et al., 2021) (Fig. 1). To assess the changes in brainwide functional connectivity following DCZ administration, we calculated functional connectivity using predetermined ROIs based on the cortical hierarchical atlas (CHARM) (Jung et al., 2021) and subcortical hierarchical atlas (SARM) (Hartig et al., 2021) for rhesus macaques (Fig. 2*A*,*C*). The *z*-transformed correlation coefficients between fMRI signal time courses in all ROIs were computed for each condition, for both the baseline (before drug injection) and test (after drug injection) scans (Fig. 2*B*,*D*, left and middle columns). Then, the difference in *z* value (test – baseline) was computed for each drug condition (Fig. 2*B*,*D*, right columns). This feature of our experimental design was important as it allowed us to control for normal session-to-session variation in fMRI signals that could influence the patterns of functional connectivity seen in the brain areas of interest following drug administration. Figure 2 shows the full matrix of correlation coefficients from this connectome-based analysis from a single subject (Monkey Bu). As expected, we found clear patterns of correlations between distinct brain areas that are consistent to previous reports in macaques (Grayson et al., 2016) in baseline scans (Fig. 2*B*, left column).

Neither vehicle (2% DMSO in saline) nor low-dose DCZ (0.1 mg/kg) administration caused a detectable change in the overall pattern of functional connectivity; consequently, there were very minor differences in functional connectivity between

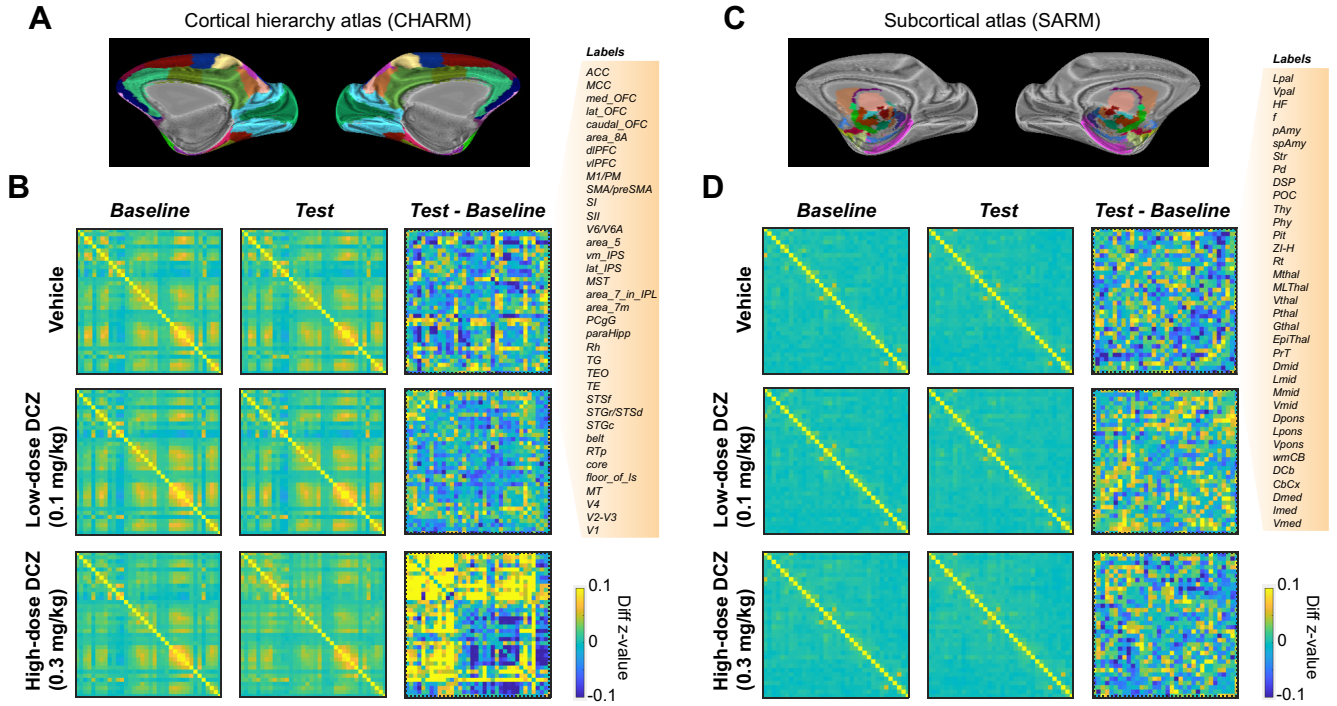


**Figure 2.** fMRI-based connectome changes after DCZ administration in an example subject. ***A***, CHARM atlas Level 3 visualized on an inflated brain (medial view). ***B***, Brainwide functional connectivity in cortical areas. Confusion matrices represent connectome in baseline scans (left column), test scans (middle column), and the difference between test and baseline (right column) for either in the vehicle (top), low-dose DCZ (middle), and high-dose DCZ condition (bottom), respectively. Color represents *z*-transformed correlation coefficients. Labels on the right side represent ROIs from CHARM atlas. ***C***, SARM atlas Level 3 visualized on an inflated brain. ***D***, Confusion matrices for subcortical areas with labels for SARM ROIs on the right side. Conventions are as in ***B***.

test and baseline scans for these conditions (Fig. 2*B*, compare top right and middle right). Conversely, high-dose DCZ administration (0.3 mg/kg) profoundly increased functional connectivity across cortical regions (Fig. 2*B*, bottom right). This effect was most apparent in frontal areas, where, compared with baseline, correlations increased, as well as between frontal cortex and other parts of the brain. In contrast to cortex, correlations between subcortical areas were not impacted by the different drug levels (Fig. 2*D*).

To assess the group-level impact of DCZ on brainwide connectomes, we computed correlation matrices for individual subjects for baseline and test scans ($N = 4$–6 subjects per condition; Table 1). Then the *z* value differences were averaged across subjects (Fig. 3). Similar to what we saw for a single subject (Fig. 2), vehicle or low-dose DCZ had little impact on overall functional connectivity. In contrast, high-dose DCZ increased functional connectivity in cortical areas but not in subcortical areas (Fig. 3*A*,*D*). Collectively, average functional connectivity was stronger in the high-dose DCZ condition compared with vehicle or low-dose DCZ in cortical areas but not in subcortical areas (Fig. 3*B*,*E*). Two-way ANOVA (Drug: vehicle, low-dose DCZ, or high-dose DCZ × Area category: cortical or subcortical areas) revealed a significant main effect of drug ($F_{(2,13\,450)} = 31$, $p = 0.0001$) and an interaction between drug and area category ($F_{(2,13\,450)} = 8.2$, $p = 0.016$). *Post hoc* analyses confirmed that high-dose DCZ modulated overall functional connectivity predominantly in cortical areas (vehicle or low-dose DCZ vs high-dose DCZ, $p < 0.0001$). The results were essentially the same when we analyzed a subset of 3 animals (Monkeys Bu, Cy, Wo) that completed all the drug conditions. In keeping with prior analyses, a two-way ANOVA conducted only on data from these 3 animals revealed a significant interaction between drug and area ($F_{(2,10\,711)} = 81.91$, $p < 0.00{,}001$).

Next, we assessed how high-dose DCZ differentially impacted functional connectivity across different lobes. Frontal, temporal, parietal, but not occipital cortex, showed marked changes in functional connectivity between the high-dose DCZ and vehicle conditions (Fig. 3*C*, bottom, $^*p < 0.01$, rank-sum test with Bonferroni correction). Furthermore, the proportion of brain areas that were impacted by low-dose DCZ was far lower than those impacted by high-dose DCZ (Fig. 3*C*, top, $\chi^2$ test, $\chi^2 = 23$, $p = 1.6 \times 10^{-6}$). Neither DCZ dose level affected functional connectivity in subcortical areas (Fig. 3*F*), suggesting the mechanism of functional connectivity changes was exclusive to cortical regions.

### Independent components (ICs) reflect brainwide functional connectivity changes caused by high-dose DCZ

While informative, the prior ROI-based approach is limited by predefined anatomic boundaries and may overlook relevant changes in MRI signals not aligned to anatomic boundaries, and does not reveal network-level changes that includes more than two areas. Thus, we performed a data-driven independent component analysis (ICA) to identify 30 ICs that are spatially coherent time courses in the whole-brain fMRI signal. We found a variety of ICs mainly located in cortical areas (Fig. 4*A*–*F*, top). To identify ICs, and thus regions that are affected by high-dose DCZ, a two-way ANOVA was performed (Drug: vehicle, low-dose or high-dose DCZ × Time: baseline or test). This analysis revealed clusters (>60 voxels with $F > 3.5$) in a subset of the ICs that showed a significant main effect of drug; these included cortical areas, such as the dorsolateral PFC, ACC, posterior cingulate cortex, ventromedial PFC, and somatosensory and motor

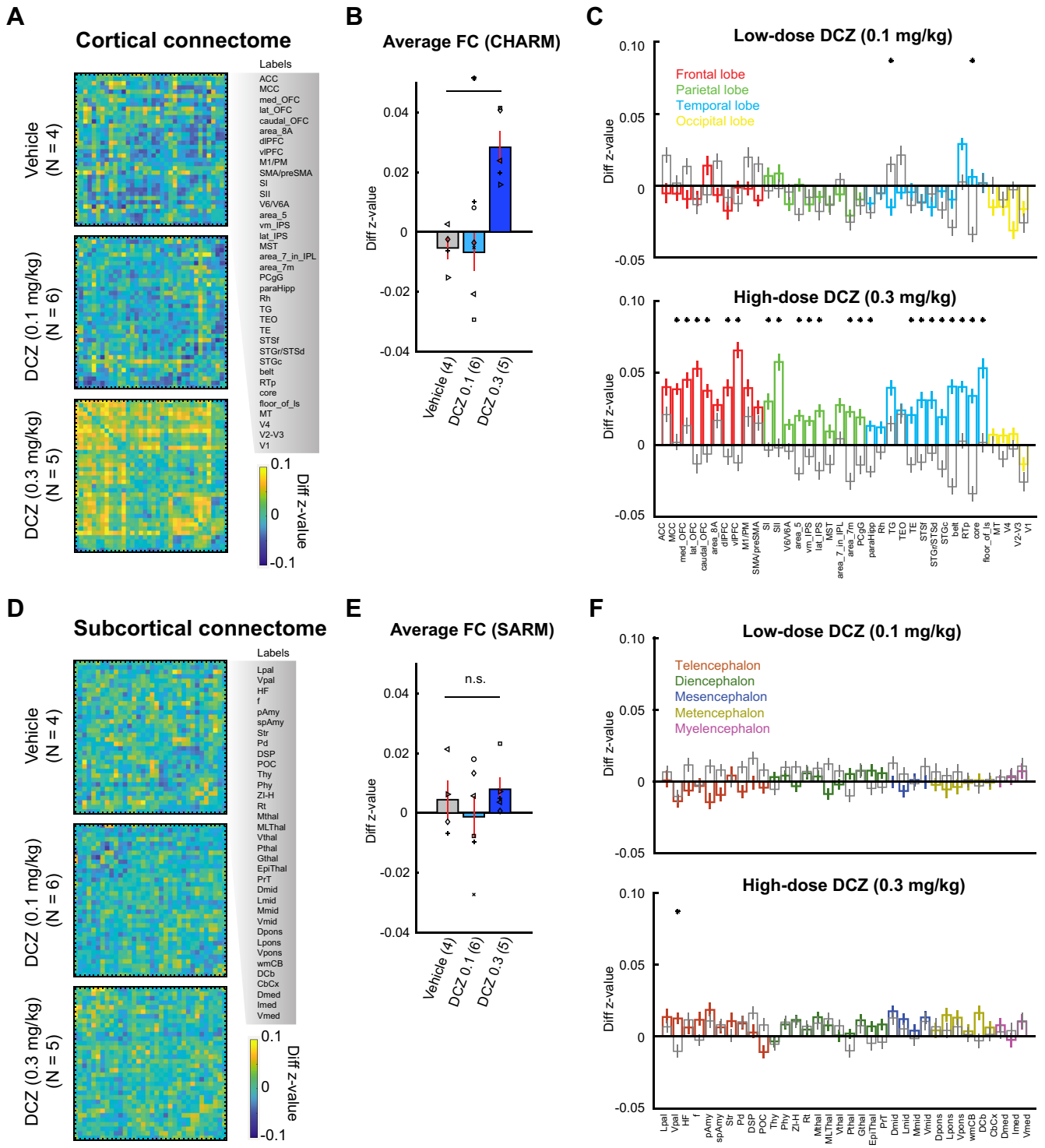


**Figure 3.** Group-level changes in the fMRI-based connectome following DCZ administration. ***A–C***, Functional connectivity changes in cortical areas. ***A***, Confusion matrices represent differences in *z* value (test − baseline) for vehicle (top), low-dose DCZ (middle), and high-dose DCZ (bottom) conditions. Labels on the right side represent ROIs from CHARM atlas (Level 3). ***B***, Averaged functional connectivity. Bars represent averaged *z* value differences for vehicle, low-dose DCZ, and high-dose DCZ conditions. Error bars indicate SE. Symbols represent subjects. $^{*}p = 0.016$, Significant interaction of drug × area category (two-way ANOVA). Numbers on the labels indicate the number of subjects for each condition. ***C***, Functional connectivity in each area. Bars represent averaged *z* value differences averaged for each area of the CHARM atlas. Colors represent frontal (red), parietal (green), temporal (cyan), and occipital areas (yellow) for low-dose (top) and high-dose (bottom) DCZ conditions. Gray bars represent vehicle condition. Error bars indicate SE. $^{*}p < 0.01$, Significant difference between vehicle and DCZ conditions (Bonferroni correction, rank-sum test). ***D–F***, Functional connectivity changes in subcortical areas. Conventions are the same as in ***A–C***. ***F***, Colors represent telencephalon (dark red), diencephalon (dark green), mesencephalon (dark blue), metencephalon (dark yellow), and myelencephalon areas (magenta).

cortices (Fig. 4*A–F*, bottom). Notably, IC three showed an effect of drug on the fronto-temporo-parietal network, implicated in mediating attentional processes (Sani et al., 2019) (Fig. 4*A*). Further, the ICs which showed drug effects overlapped with regions that showed increased functional connectivity in our ROI-based analyses (Fig. 3). Systemic administration of high-dose DCZ influenced brainwide spatially coherent patterns of neural activity, especially in attentionally-linked fronto-temporo-parietal circuits.

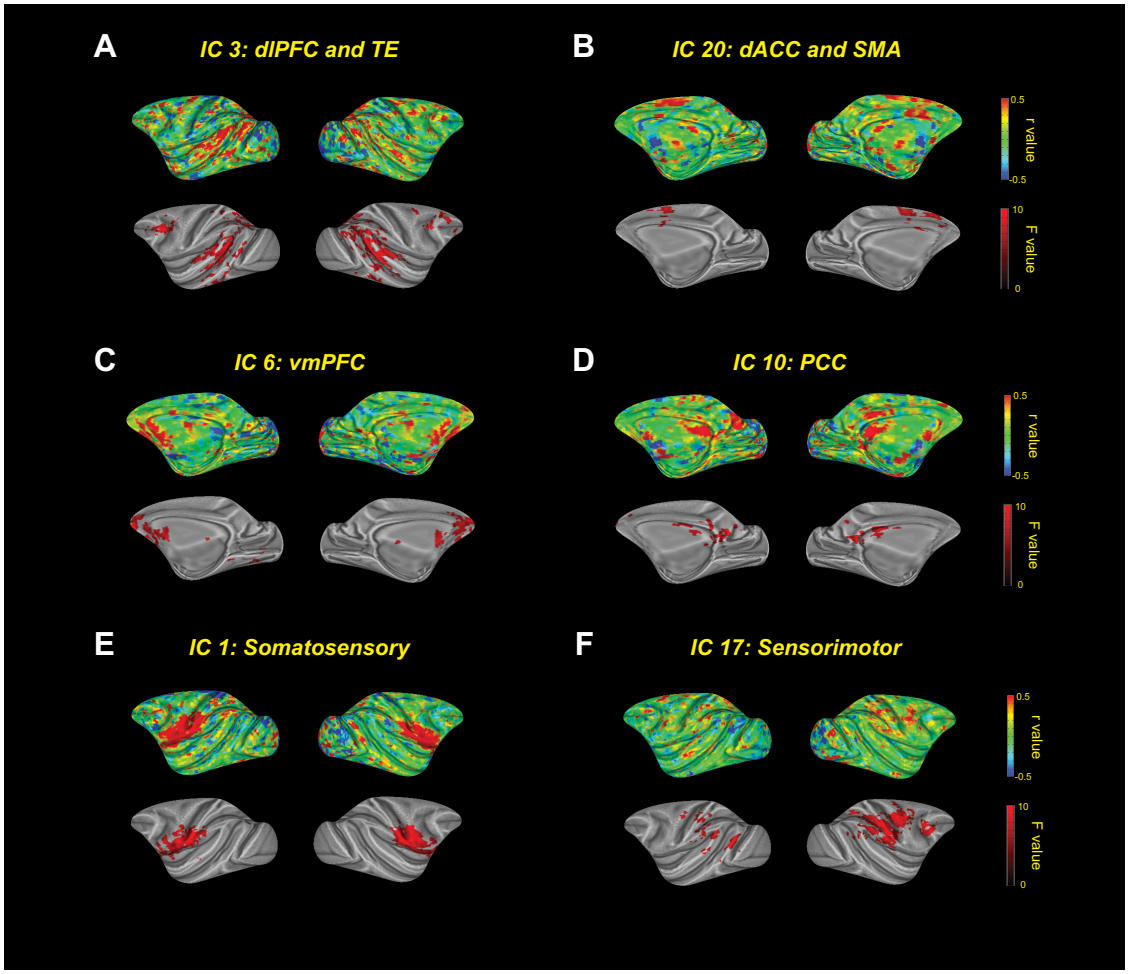


**Figure 4.** ICA of the effect of high-dose DCZ. ***A–F***, Top panels, ICs as correlation coefficients (*r*) on inflated brains. Bottom panels, Clusters that showed a significant main effect of drug condition ($p < 0.05$, two-way ANOVA).

**Negligible effects of low-dose DCZ on socio-emotional behaviors**

Our imaging results demonstrated a negligible impact of 0.1 mg/kg DCZ on brainwide functional connectivity with the least impact in subcortical structures (Fig. 3). Although no adverse effects of low-dose DCZ were reported in a working-memory task in macaque monkeys (Nagai et al., 2020; Upright and Baxter, 2020), no study has examined the impact of DCZ on the socio-emotional responses of monkeys. To address this issue, a subset of 4 subjects were assessed in the human intruder task, a well-validated socio-emotional task for nonhuman primates (Kling and Cornell, 1971; Kalin and Shelton, 1989). Subjects received an intramuscular injection of either low-dose DCZ or vehicle before testing. We analyzed the time spent motionless on each trial type (alone, profile, or stare condition) as a measure of anxiety-like behavior. We expected that the animals spent more time motionless in the "profile" condition in response to indirect threat compared with the "alone" or directly threatening "stare" condition (Kalin and Shelton, 1989). Animals did spend more time motionless in the "profile" condition in both vehicle and low-dose DCZ conditions (Fig. 5*A*). A two-way ANOVA matched for subject (Trial type: alone, profile, or stare × Drug: vehicle or low-dose DCZ) revealed a significant main effect of trial type ($F_{(1,3)} = 16$, $\eta^2 = 0.56$, $p = 0.049$), but no main effect of drug ($F_{(1,3)} = 0.24$, $\eta^2 = 0.0048$, $p = 0.66$) nor an interaction between trial type and drug ($F_{(2,6)} = 1.4$, $\eta^2 = 0.0086$, $p = 0.32$). We also analyzed the frequency of anxious and hostile behaviors during the threatening stare condition. There were no differences between low-dose DCZ and vehicle for either anxiety behaviors (mean ± SD, vehicle: 10.5 ± 9.6 and low-dose DCZ: 24.8 ± 35.7, respectively; $t = 0.68$, $p = 0.54$, paired *t* test) or hostile behaviors (mean ± SD, vehicle: 28.3 ± 32.1 and low-dose DCZ: 37.5 ± 43.4, respectively; $t = 1.49$, $p = 0.23$, paired *t* test).

We also examined whether low-dose DCZ alters social interaction. Subjects were paired with a cagemate, and the total social contact, comprising grooming, play, and passive physical contact, was measured (Kling and Cornell, 1971). There were no statistical differences between vehicle and low-dose DCZ conditions on these measures (mean ± SD, vehicle: 435.4 ± 198.2 s and low-dose DCZ: 502.1 ± 342.3 s, respectively; $t = 0.26$, $p = 0.81$, paired *t* test). Thus, we found no evidence that macaque socio-emotional behaviors were affected by systemic administration of low-dose DCZ.

**Effect of high-dose DCZ on decision-making and its relation to resting-state functional connectivity**

Our imaging results revealed an increase in overall functional connectivity in cortical areas following a systemic administration of high-dose DCZ (0.3 mg/kg) (Figs. 3 and 4). Because the changes occurred mainly in frontal, temporal, and parietal cortex, it likely influences behaviors dependent on functional interaction between these areas (Fig. 4). We trained a subset of 3 monkeys in a translationally relevant probabilistic learning task that relies on frontal

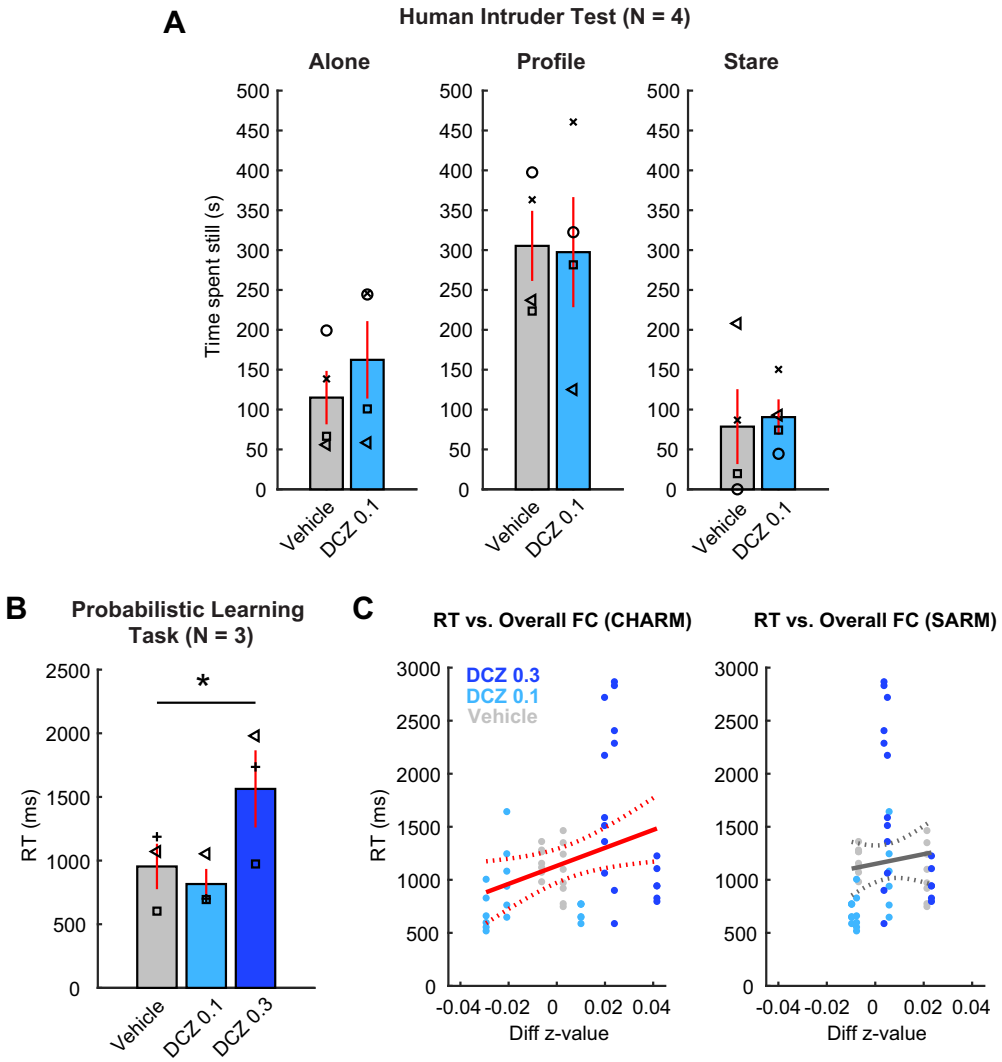


**Figure 5.** The impact of systemic DCZ administration on socio-emotional behavior and probabilistic learning. ***A***, The effect of low-dose DCZ in the human intruder task. Bars represent the mean time spent motionless with systemic administration of vehicle (gray) or low-dose DCZ (light blue) in alone condition (left), profile condition (middle), or stare condition (right). Symbols represent individual animals. Error bars indicate SE. ***B***, Dosage-dependent changes in RT in the probabilistic learning task. Bar plots represent the mean RT of 3 subjects in each drug condition (vehicle, low-dose DCZ, high-dose DCZ). Error bars indicate SE. Symbols represent individual subjects. *Significant main effect of drug condition ($p = 2.5 \times 10^{-6}$, one-way repeated-measures ANOVA). ***C***, Relationship between RT and functional connectivity across conditions in the probabilistic learning task. Scatter plots represent the RT in each behavioral session (*y* axis) and the change in overall functional connectivity in a corresponding subject (*x* axis) for cortical areas (left) and for subcortical areas (right), respectively. Individual monkeys completed 6-8 behavioral sessions per each condition. Colors represent drug conditions. Solid and dotted lines indicate linear fitting and CIs, respectively. Red lines indicate significant linear correlation between RT and *z* value ($p = 0.023$).

and temporal cortices (Pizzagalli et al., 2008; Chau et al., 2015; Rudebeck et al., 2017). We theorized that high-dose DCZ would specifically increase monkeys' RT as the drug slows decision-making. RTs did increase after high-dose DCZ but not low-dose DCZ, compared with vehicle (Fig. 5*B*). A one-way repeated-measures ANOVA (Drug: vehicle, low-dose DCZ, or high-dose DCZ) revealed a significant main effect of drug ($F_{(2,49)} = 17$, $\eta^2 = 0.49$, $p = 2.5 \times 10^{-6}$), suggesting that high-dose DCZ causes an impairment in general task-execution processes, while low-dose DCZ did not. Based on these results, we did not include a high-dose DCZ condition in the socioemotional tasks. This was because an impairment on the socioemotional tasks could simply be the result of a change in attentional function, complicating interpretation of the results.

To analyze the relationship between the neural and behavioral effects following systemic DCZ, we correlated overall functional connectivity changes in cortical (Fig. 5*C*, left) or subcortical areas (Fig. 5*C*, right) with RT in the 3 animals. There was a significant positive correlation between RT and cortical functional connectivity ($n = 58$, $p = 0.023$) but no correlation with subcortical areas ($n = 58$, $p = 0.49$), suggesting that cortical resting-state changes following DCZ administration were related to the impairment in task-execution process observed after high-dose DCZ.

## Discussion

To assess the impact of DCZ on brainwide function in primates, we conducted rs-fMRI experiments and behavioral assessments in macaque monkeys. We found that systemic administration of low-dose DCZ (0.1 mg/kg) did not affect overall functional connectivity or the socio-emotional behaviors we measured. However, we did find that systemic administration of high-dose DCZ (0.3 mg/kg) increased overall cortical functional connectivity, and was associated with slowed responses in a probabilistic learning task. Together, our data indicate that, at a functionally effective dose of 0.1 mg/kg, DCZ appears to be appropriate for use as a

DREADD actuator in nonhuman primates, a key finding if chemogenetics are to be translated further.

### Negligible impact of low-dose DCZ on brainwide functional connectivity or socio-emotional behaviors

Although DCZ was identified as a potent, selective, and metabolically stable DREADD actuator (Nagai et al., 2020), prior work only showed its local effects on the brain using electrophysiology and [18F] FDG-PET imaging (Nagai et al., 2020). What was not clear is whether it impacts brainwide neural activity in normal controls where DREADD receptors are not present. Consequently, we conducted an rs-fMRI experiment with 7 rhesus monkeys and assessed the effect of different dose levels of DCZ. Animals were only lightly anesthetized throughout the scan sessions so that the resting-state brain activity was preserved as close to that of the awake state as possible (Hutchison et al., 2013; Wu et al., 2016; Giacometti et al., 2021). We hypothesized that low-dose DCZ, which is functionally effective in chemogenetic experiments in nonhuman primates (Nagai et al., 2020; Hirabayashi et al., 2021), would not affect resting-state functional connectivity in non-transfected animals. As we expected, low-dose DCZ did not alter brainwide functional connectivity either in cortical or subcortical areas (Figs. 2 and 3).

Although DCZ has a high-degree of selectivity to DREADD receptors, it shows some affinity to endogenous mAchR and serotonin receptors (Nagai et al., 2020). Past studies demonstrated a negligible effect of low-dose DCZ on performance in a working-memory task in control monkeys (Nagai et al., 2020; Upright and Baxter, 2020), suggesting that this dose of DCZ does not affect working memory performance or attention, processes linked to mAchR (Kuczewski et al., 2005). In the current study, we assessed socio-emotional functions of monkeys in the human intruder and social interaction tasks (Kling and Cornell, 1971; Kalin and Shelton, 1989), which are likely mediated by the serotonergic system (Broekkamp et al., 1989; Santangelo et al., 2016, 2019; Weinberg-Wolf and Chang, 2019). We asked whether even subtle agonism to endogenous serotonin receptors by DCZ might impact unconditioned affective behaviors. Our results indicate that systemic low-dose DCZ did not modify affective behaviors of the monkeys (Fig. 5). In summary, there is a negligible effect of low-dose DCZ on socio-emotional functions or brainwide functional connectivity.

### Functional connectivity changes following high-dose DCZ administration

Systemic administration of high-dose, 0.3 mg/kg, DCZ occupies nearly 100% of DREADD receptors when administered in monkeys expressing DREADDs in their brain (Nagai et al., 2020). The question remained as to whether high-dose DCZ also causes significant nonspecific binding of endogenous receptors leading to neural and behavioral alterations. Indeed, DCZ at this dosage reduces performance in a working-memory task, suggesting that the excess DCZ affects neural activity (Upright and Baxter, 2020). Our imaging results revealed that high-dose DCZ caused a prominent increase in overall resting-state functional connectivity between frontal, temporal, and parietal lobes that was not observed for vehicle or low-dose DCZ (Figs. 2 and 3). Notably, the changes were mainly observed in networks that include frontal regions, and no obvious effects were observed in occipital cortex or subcortical structures. This coincides with the pattern of serotonin Type 2 receptor ($5\text{-HT}_{2A}$, $5\text{-HT}_{2C}$) expression in the brain (Mengod et al., 2006; Beliveau et al., 2017), suggesting that excess DCZ may alter brain function through binding to endogenous serotonin receptors.

### Behavioral changes following high-dose DCZ administration were associated with functional connectivity changes

While low-dose DCZ has little impact on behavior, higher dose levels were associated with behavioral changes. Specifically, high-dose DCZ significantly increased RT in the probabilistic learning task compared with other drug conditions, indicating an impairment in general task-execution processes, such as attention (Fig. 5). Our ICA results revealed a prominent drug effect in a fronto-temporo-parietal network (IC 3, Fig. 4), heavily linked to attentional processes (Sani et al., 2019). Alternatively, high-dose DCZ may increase RT by affecting motivation; this seems less likely, as motivation is largely mediated by subcortical circuits (Robbins and Everitt, 1996).

Past studies have demonstrated that patterns of rs-fMRI functional connectivity in humans are directly related to subsequent behavioral measures recorded in separate sessions (Li et al., 2013; Kohno et al., 2014). Consistently, we found that the changes in cortical functional connectivity and RT were positively correlated (Fig. 5). This increase in cortical functional connectivity mirrors the slowing of responses that may seem counterintuitive as one could expect an improvement in task performance as a result of increased functional connectivity. However, rs-fMRI functional connectivity reflects low-frequency fluctuations of neural activity between brain regions, and broad, multiregion, increases in functional connectivity do not necessarily benefit coordinated activity across distributed areas (Hillary and Grafman, 2017). Our data suggest that hyperconnectivity in frontal regions could underlie the impairments in attention that are prominent in neurologic and psychiatric disorders (Zhou et al., 2010; Di Martino et al., 2011; Siegel et al., 2016).

### Resting-state MRI as a tool for benchmarking in chemogenetic experiments and drug screening

Primate chemogenetic technique development has been relatively slow for a number of reasons, including the limited number of animals available for development and physiological differences between rodents and primates that hampers viral delivery (Fredericks et al., 2019; Albaugh et al., 2020). Although PET imaging is useful for the quantification of chemogenetic receptor expression *in vivo* (Nagai et al., 2016; Bonaventura et al., 2019; Nagai et al., 2020), the more accessible rs-fMRI should play a complementary role. Here we show that rs-fMRI provides insight into the correlated patterns of neural activity across distinct brain areas and how this can be impacted by pharmacological agents, a level of analysis unavailable with PET. Thus, rs-fMRI has advantages for screening chemogenetic actuators in naive animals without specific task training. Moreover, rs-fMRI is potentially useful for "benchmarking" the selectivity and potency of novel chemogenetic actuators (Milham et al., 2022), accelerating the development of chemogenetics in primates.

In the present study, we minimized session-by-session variance in functional connectivity by carefully controlling anesthesia level and by subtracting within-session baseline scans from post-drug injection scans. Although the variance across the conditions was small and within the normal range of resting-state MRI functional connectivity, future studies should be conducted with larger cohorts to specifically investigate the interaction between individual differences and DCZ. Additionally, the animals used in this study were all close in age and included only 1 female; thus, an analysis of the effect of DCZ by age and/or sex

differences is beyond the scope of this study. However, future studies with larger cohorts of animals should address this issue as it is critical to understand dose-dependent effects.

In conclusion, the present study demonstrated that DCZ is inert in non-DREADD monkeys both in brainwide activity and in conditioned and unconditioned behaviors, if the dosage is carefully controlled. We also highlight a link between resting-state hyperconnectivity and behavioral impairments, providing a neural mechanism underlying the side effects caused by excess DCZ. Our data underscore the value of fMRI to accelerate the development of chemogenetics in primates, research that is essential for the translation of these approaches to treat human psychiatric disorders.

## References


Albaugh DL, Smith Y, Galvan A (2020) Comparative analyses of transgene expression patterns after intra-striatal injections of rAAV2-retro in rats and rhesus monkeys: a light and electron microscopic study. Eur J Neurosci 52:4824–4839.

Armbruster BN, Li X, Pausch MH, Herlitze S, Roth BL (2007) Evolving the lock to fit the key to create a family of G protein-coupled receptors potently activated by an inert ligand. Proc Natl Acad Sci USA 104:5163–5168.

Barnes NM, Sharp T (1999) A review of central 5-HT receptors and their function. Neuropharmacology 38:1083–1152.

Beckmann CF, Smith SM (2004) Probabilistic independent component analysis for functional magnetic resonance imaging. IEEE Trans Med Imaging 23:137–152.

Beckmann CF, Mackay CE, Filippini N, Smith SM (2009) Group comparison of resting-state FMRI data using multi-subject ICA and dual regression. Neuroimage 47:S148.

Beliveau V, Ganz M, Feng L, Ozenne B, Højgaard L, Fisher PM, Svarer C, Greve DN, Knudsen GM (2017) A high-resolution in vivo atlas of the human brain's serotonin system. J Neurosci 37:120–128.

Bonaventura J, et al. (2019) High-potency ligands for DREADD imaging and activation in rodents and monkeys. Nat Commun 10:4627.

Broekkamp CL, Berendsen HH, Jenck F, Van Delft AM (1989) Animal models for anxiety and response to serotonergic drugs. Psychopathology 22:2–12.

Chau BK, Sallet J, Papageorgiou GK, Noonan MP, Bell AH, Walton ME, Rushworth MF (2015) Contrasting roles for orbitofrontal cortex and amygdala in credit assignment and learning in macaques. Neuron 87:1106–1118.

Cox RW (1996) AFNI: software for analysis and visualization of functional magnetic resonance neuroimages. Comput Biomed Res 29:162–173.

Di Martino A, Kelly C, Grzadzinski R, Zuo XN, Mennes M, Mairena MA, Lord C, Castellanos FX, Milham MP (2011) Aberrant striatal functional connectivity in children with autism. Biol Psychiatry 69:847–856.

Forcelli PA, Wellman LL, Malkova L (2017) Blockade of glutamatergic transmission in the primate basolateral amygdala suppresses active behavior without altering social interaction. Behav Neurosci 131:192–200.

Fredericks JM, Fujimoto A, Rudebeck PH (2019) Trust, but verify: a cautionary tale of translating chemogenetic methods (a commentary on Galvan et al). Eur J Neurosci 50:2751–2754.

Giacometti C, Dureux A, Autran-Clavagnier D, Wilson CR, Sallet J, Dirheimer M, Procyk E, Hadj-Bouziane F, Amiez C (2021) Frontal cortical functional connectivity is impacted by anaesthesia in macaques. Cereb Cortex. Available at https://doi.org/10.1093/cercor/bhab465.

Gomez JL, Bonaventura J, Lesniak W, Mathews WB, Sysa-Shah P, Rodriguez LA, Ellis RJ, Richie CT, Harvey BK, Dannals RF, Pomper MG, Bonci A, Michaelides M (2017) Chemogenetics revealed: DREADD occupancy and activation via converted clozapine. Science 357:503–507.

Gorgolewski KJ, et al. (2016) The brain imaging data structure, a format for organizing and describing outputs of neuroimaging experiments. Sci Data 3:160044.

Grayson DS, Bliss-Moreau E, Machado CJ, Bennett J, Shen K, Grant KA, Fair DA, Amaral DG (2016) The rhesus monkey connectome predicts disrupted functional networks resulting from pharmacogenetic inactivation of the amygdala. Neuron 91:453–466.

Hartig R, Glen D, Jung B, Logothetis NK, Paxinos G, Garza-Villarreal EA, Messinger A, Evrard HC (2021) The Subcortical Atlas of the Rhesus Macaque (SARM) for neuroimaging. Neuroimage 235:117996.

Hillary FG, Grafman JH (2017) Injured brains and adaptive networks: the benefits and costs of hyperconnectivity. Trends Cogn Sci 21:385–401.

Hirabayashi T, Nagai Y, Hori Y, Inoue KI, Aoki I, Takada M, Suhara T, Higuchi M, Minamimoto T (2021) Chemogenetic sensory fMRI reveals behaviorally relevant bidirectional changes in primate somatosensory network. Neuron 109:3312–3322.e3315.

Hutchison RM, Womelsdorf T, Gati JS, Everling S, Menon RS (2013) Resting-state networks show dynamic functional connectivity in awake humans and anesthetized macaques. Hum Brain Mapp 34:2154–2177.

Izquierdo A, Newman TK, Higley JD, Murray EA (2007) Genetic modulation of cognitive flexibility and socioemotional behavior in rhesus monkeys. Proc Natl Acad Sci USA 104:14128–14133.

Jung B, Taylor PA, Seidlitz J, Sponheim C, Perkins P, Ungerleider LG, Glen D, Messinger A (2021) A comprehensive macaque fMRI pipeline and hierarchical atlas. Neuroimage 235:117997.

Kalin NH, Shelton SE (1989) Defensive behaviors in infant rhesus monkeys: environmental cues and neurochemical regulation. Science 243:1718–1721.

Kalin NH, Shelton SE, Davidson RJ, Kelley AE (2001) The primate amygdala mediates acute fear but not the behavioral and physiological components of anxious temperament. J Neurosci 21:2067–2074.

Kalin NH, Shelton SE, Davidson RJ (2007) Role of the primate orbitofrontal cortex in mediating anxious temperament. Biol Psychiatry 62:1134–1139.

Kling A, Cornell R (1971) Amygdalectomy and social behavior in the caged stump-tailed macaque (*Macaca speciosa*). Folia Primatol (Basel) 14:190–208.

Kohno M, Morales AM, Ghahremani DG, Hellemann G, London ED (2014) Risky decision making, prefrontal cortex, and mesocorticolimbic functional connectivity in methamphetamine dependence. JAMA Psychiatry 71:812–820.

Kuczewski N, Aztiria E, Gautam D, Wess J, Domenici L (2005) Acetylcholine modulates cortical synaptic transmission via different muscarinic receptors, as studied with receptor knockout mice. J Physiol 566:907–919.

Leite FP, Tsao D, Vanduffel W, Fize D, Sasaki Y, Wald LL, Dale AM, Kwong KK, Orban GA, Rosen BR, Tootell RB, Mandeville JB (2002) Repeated fMRI using iron oxide contrast agent in awake, behaving macaques at 3 Tesla. Neuroimage 16:283–294.

Li N, Ma N, Liu Y, He XS, Sun DL, Fu XM, Zhang X, Han S, Zhang DR (2013) Resting-state functional connectivity predicts impulsivity in economic decision-making. J Neurosci 33:4886–4895.

Mengod G, Vilaró MT, Cortés R, López-Giménez JF, Raurich A, Palacios JM (2006) Chemical Neuroanatomy of 5-HT Receptor Subtypes in the Mammalian Brain. In: Roth, B.L. (eds) The Serotonin Receptors. The Receptors. Humana Press. https://doi.org/10.1007/978-1-59745-080-5_10.

Milham M, et al. (2022) Toward next-generation primate neuroscience: a collaboration-based strategic plan for integrative neuroimaging. Neuron 110:16–20.

Nagai Y, et al. (2016) PET imaging-guided chemogenetic silencing reveals a critical role of primate rostromedial caudate in reward evaluation. Nat Commun 7:13605.

Nagai Y, et al. (2020) Deschloroclozapine, a potent and selective chemogenetic actuator, enables rapid neuronal and behavioral modulations in mice and monkeys. Nat Neurosci 23:1157–1167.

Nickerson LD, Smith SM, Öngür D, Beckmann CF (2017) Using dual regression to investigate network shape and amplitude in functional connectivity analyses. Front Neurosci 11:115.

Pizzagalli DA, Iosifescu D, Hallett LA, Ratner KG, Fava M (2008) Reduced hedonic capacity in major depressive disorder: evidence from a probabilistic reward task. J Psychiatr Res 43:76–87.

Raper J, Murphy L, Richardson R, Romm Z, Kovacs-Balint Z, Payne C, Galvan A (2019) Chemogenetic inhibition of the amygdala modulates emotional behavior expression in infant rhesus monkeys. eNeuro 6: ENEURO.0360-19.2019.

Robbins TW, Everitt BJ (1996) Neurobehavioural mechanisms of reward and motivation. Curr Opin Neurobiol 6:228–236.

Rodd ZA, Engleman EA, Truitt WA, Burke AR, Molosh AI, Bell RL, Hauser SR (2022) CNO administration increases dopamine and glutamate in the medial prefrontal cortex of Wistar rats: further concerns for the validity of the CNO-activated DREADD procedure. Neuroscience 491:176–184.

Roseboom PH, Mueller SA, Oler JA, Fox AS, Riedel MK, Elam VR, Olsen ME, Gomez JL, Boehm MA, DiFilippo AH, Christian BT, Michaelides M, Kalin NH (2021) Evidence in primates supporting the use of chemogenetics for the treatment of human refractory neuropsychiatric disorders. Mol Ther 29:3484–3497.

Roth BL (2016) DREADDs for neuroscientists. Neuron 89:683–694.

Rudebeck PH, Saunders RC, Lundgren DA, Murray EA (2017) Specialized representations of value in the orbital and ventrolateral prefrontal cortex: desirability versus availability of outcomes. Neuron 95:1208–1220.e1205.

Russ BE, Petkov CI, Kwok SC, Zhu Q, Belin P, Vanduffel W, Hamed SB (2021) Common functional localizers to enhance NHP and cross-species neuroscience imaging research. Neuroimage 237:118203.

Sani I, McPherson BC, Stemmann H, Pestilli F, Freiwald WA (2019) Functionally defined white matter of the macaque monkey brain reveals a dorso-ventral attention network. Elife 8:e40520.

Santangelo AM, Ito M, Shiba Y, Clarke HF, Schut EH, Cockcroft G, Ferguson-Smith AC, Roberts AC (2016) Novel primate model of serotonin transporter genetic polymorphisms associated with gene expression, anxiety and sensitivity to antidepressants. Neuropsychopharmacology 41:2366–2376.

Santangelo AM, Sawiak SJ, Fryer T, Hong Y, Shiba Y, Clarke HF, Riss PJ, Ferrari V, Tait R, Suckling J, Aigbirhio FI, Roberts AC (2019) Insula serotonin 2A receptor binding and gene expression contribute to serotonin transporter polymorphism anxious phenotype in primates. Proc Natl Acad Sci USA 116:14761–14768.

Seidlitz J, Sponheim C, Glen D, Ye FQ, Saleem KS, Leopold DA, Ungerleider L, Messinger A (2018) A population MRI brain template and analysis tools for the macaque. Neuroimage 170:121–131.

Siegel JS, Ramsey LE, Snyder AZ, Metcalf NV, Chacko RV, Weinberger K, Baldassarre A, Hacker CD, Shulman GL, Corbetta M (2016) Disruptions of network connectivity predict impairment in multiple behavioral domains after stroke. Proc Natl Acad Sci USA 113:E4367–E4376.

Stachniak TJ, Ghosh A, Sternson SM (2014) Chemogenetic synaptic silencing of neural circuits localizes a hypothalamus→midbrain pathway for feeding behavior. Neuron 82:797–808.

Taylor PA, Saad ZS (2013) FATCAT: (an efficient) Functional and Tractographic Connectivity Analysis Toolbox. Brain Connect 3:523–535.

Upright NA, Baxter MG (2020) Effect of chemogenetic actuator drugs on prefrontal cortex-dependent working memory in nonhuman primates. Neuropsychopharmacology 45:1793–1798.

Varastet M, Brouillet E, Chavoix C, Prenant C, Crouzel C, Stulzaft O, Bottlaender M, Cayla J, Mazière B, Mazière M (1992) In vivo visualization of central muscarinic receptors using [11C]quinuclidinyl benzilate and positron emission tomography in baboons. Eur J Pharmacol 213:275–284.

Wang X, Li XH, Cho JW, Russ BE, Rajamani N, Omelchenko A, Ai L, Korchmaros A, Sawiak S, Benn RA, Garcia-Saldivar P, Wang Z, Kalin NH, Schroeder CE, Craddock RC, Fox AS, Evans AC, Messinger A, Milham MP, Xu T (2021) U-net model for brain extraction: trained on humans for transfer to non-human primates. Neuroimage 235:118001.

Weinberg-Wolf H, Chang SW (2019) Differences in how macaques monitor others: does serotonin play a central role? Wiley Interdiscip Rev Cogn Sci 10:e1494.

Wellman LL, Forcelli PA, Aguilar BL, Malkova L (2016) Bidirectional control of social behavior by activity within basolateral and central amygdala of primates. J Neurosci 36:8746–8756.

Wu TL, Mishra A, Wang F, Yang PF, Gore JC, Chen LM (2016) Effects of isoflurane anesthesia on resting-state fMRI signals and functional connectivity within primary somatosensory cortex of monkeys. Brain Behav 6:e00591.

Zhou J, Greicius MD, Gennatas ED, Growdon ME, Jang JY, Rabinovici GD, Kramer JH, Weiner M, Miller BL, Seeley WW (2010) Divergent network connectivity changes in behavioural variant frontotemporal dementia and Alzheimer's disease. Brain 133:1352–1367.